PNAS RESEARCH ARTICLE | PHYSICS

Discontinuous instabilities in disordered solids

Ding Xu[a], Shiyun Zhang[a], Andrea J. Liu[b,c], Sidney R. Nagel[d], and Ning Xu[a,1]

Edited by Pablo Debenedetti, Princeton University, Princeton, NJ; received March 26, 2023; accepted July 26, 2023

Under a sufficiently large load, a solid material will flow via rearrangements, where particles change neighbors. Such plasticity is most easily described in the athermal, quasistatic limit of zero temperature and infinitesimal loading rate, where rearrangements occur only when the system becomes mechanically unstable. For disordered solids, the instabilities marking the onset of rearrangements have long been believed to be fold instabilities, in which an energy barrier disappears and the frequency of a normal mode of vibration vanishes continuously. Here, we report that there exists another, anomalous, type of instability caused by the breaking of a "stabilizing bond," whose removal creates an unstable vibrational mode. For commonly studied systems, such as those with harmonic finite-range interparticle interactions, such "discontinuous instabilities" are not only inevitable, they often dominate the modes of failure. Stabilizing bonds are a subset of all the bonds in the system and are prevalent in disordered solids generally. Although they do not trigger discontinuous instabilities in systems with vanishing stiffness at the interaction cutoff, they are, even in those cases, local indicators of incipient mechanical failure. They therefore provide an accurate structural predictor of instabilities not only of the discontinuous type but of the fold type as well.

disordered solids | instability | normal mode of vibration

Significance

Plasticity (flow) in solids is studied most cleanly at zero temperature and infinitesimal loading rate. In this athermal, quasistatic limit, plasticity occurs when the system becomes unstable. It has long been believed that the instabilities are always associated with continuous vanishing of the frequency of a normal mode of vibration ("fold instabilities"). Here, we show that for certain interaction potentials, there is a second class of instabilities, which we call "discontinuous instabilities." This instability is associated with discontinuous destabilization of a vibrational mode, due to breaking of one of a class of bonds that we call "stabilizing bonds." Such bonds appear to be associated with rearrangements in a wide class of disordered solids.

At zero temperature, under external load such as shear or compression applied at an infinitesimal rate, disordered solids undergo instabilities signaled by an abrupt drop of shear stress or pressure (1–6). Understanding such instabilities is critical to understanding how disordered solids flow and predicting where they fail (7–18). It also is important for exploring how an external load forces disordered solids to traverse the complex energy landscape consisting of extensive numbers of metastable local minima (3, 6, 19–24).

Instabilities in solids have generally been understood to occur when a barrier between two adjacent energy basins disappears as the solid is put under an external load; in the absence of an energy barrier, the system transitions spontaneously to the lower-energy configuration. Because the frequencies of normal modes of vibration, ω, measure the curvatures of the energy surface, the vanishing of such a barrier implies that the lowest-frequency mode becomes soft (*i.e.*, $\omega = 0$), vanishing as a power law as the system is driven toward the instability. This is known as a fold instability (6, 13, 25).

Here, we report that, for a potential widely used to study disordered solids made up of frictionless particles, namely the purely repulsive harmonic potential, a different, unrecognized type of instability also exists and outnumbers the fold instability. Such harmonic potentials are commonly used to model contact forces and are found to be applicable in a number of experimental situations (26–29). This instability is always triggered by the breaking of a bond (so that the interaction between two particles vanishes). In contrast to the fold instability scenario, on approaching this instability, both the frequency of the lowest vibrational mode and the elastic modulus remain constant and nonvanishing, and the particle displacements do not follow any single normal mode of vibration.

We show that there are two necessary conditions for this type of instability to occur. First, the second derivative of the interaction potential, i.e., the stiffness of the bond, must be nonzero at the cutoff of the interaction. Second, the breaking bond must be a "stabilizing bond," defined as one necessary to maintain the stability of the packing. When a stabilizing bond is removed, an unstable mode is produced, causing a discontinuous instability.

We further demonstrate that the concept of stabilizing bonds generally exist for arbitrary potentials, and that the locations of the stabilizing bonds are strongly correlated with the locations of soft spots (15–18), i.e., small clusters of particles prone to rearrange under load. Stabilizing bonds are thus predictors of the microscopic location of mechanical failure under load in disordered solids generally, independent of the interaction potential.

Author affiliations: [a]Hefei National Research Center for Physical Sciences at the Microscale, Chinese Academy of Sciences Key Laboratory of Microscale Magnetic Resonance, and Department of Physics, University of Science and Technology of China, Hefei 230026, People's Republic of China; [b]Department of Physics and Astronomy, University of Pennsylvania, Philadelphia, PA 19104; [c]Center for Computational Biology, Flatiron Institute, Simons Foundation, New York, NY 10010; and [d]Department of Physics and James Franck and Enrico Fermi Institutes, University of Chicago, Chicago, IL 60637

Author contributions: A.J.L., S.R.N., and N.X. designed research; D.X. performed research; D.X., S.Z., A.J.L., S.R.N., and N.X. analyzed data; and D.X., A.J.L., S.R.N., and N.X. wrote the paper.

The authors declare no competing interest.

This article is a PNAS Direct Submission.

[1]To whom correspondence may be addressed. Email: ningxu@ustc.edu.cn.

This article contains supporting information online at https://www.pnas.org/lookup/suppl/doi:10.1073/pnas.2304974120/-/DCSupplemental.

Published August 16, 2023.

Fold Instabilities. We first outline the physics of the fold instability, which informs our understanding of instabilities in disordered solids (3, 5). Consider an instability that occurs at an applied stress τ_c. At a stress $\tau < \tau_c$ prior to the instability, assume that the energy $H(x)$ along the "reaction coordinate" x in configurational space can be approximated by

$$H(x) = -\frac{1}{3}a_3x^3 + cx\delta\tau, \quad [1]$$

where $a_3 > 0$ quantifies the anharmonicity, $\delta\tau = \tau_c - \tau$, and $c > 0$ is the coupling constant. By expanding $H(x)$ around $x = x_0 = -\sqrt{c\delta\tau/a_3}$, where $H(x)$ reaches the minimum, we have

$$H(x) = \frac{2}{3}a_3x_0^3 - a_3x_0(x-x_0)^2 - \frac{1}{3}a_3(x-x_0)^3 + \mathcal{O}[(x-x_0)^4]. \quad [2]$$

Therefore, on approaching the instability, the coefficient of the harmonic term in Eq. **2** sets the local curvature of $H(x)$ at $x = x_0$ and hence a frequency associated with the instability,

$$\omega_c = \sqrt{-2a_3x_0} \sim (\delta\tau)^{1/4}. \quad [3]$$

Meanwhile, the anharmonicity of $H(x)$ leads to an energy barrier height

$$\Delta H = \frac{1}{6}\frac{\omega_c^6}{a_3^2} \sim (\delta\tau)^{3/2}. \quad [4]$$

It has been verified in simulations (1, 5, 11, 13) that near the instability, the particle displacements under load follow the lowest normal mode of vibration with frequency ω_m, so that $\omega_c = \omega_m$. Likewise, the frequency ω_m and the energy barrier height ΔH along the lowest normal mode exhibit the scalings of Eqs. **3** and **4** and the shear (bulk) modulus decays to zero at the instability under shear (compression) (3, 5, 6, 11–13, 30).

Disordered solids have complex energy landscapes with many saddles and local minima, so an expansion around a saddlepoint as in the fold instability has been viewed as a generic description of instabilities.

Here, we only show results of instabilities under shear. We have verified that instabilities under compression behave similarly (shown in *SI Appendix*). Consider a jammed packing of N particles located at $(\mathbf{R}_0, \gamma_0)$, which is a local minimum of $H(\mathbf{R}, \gamma)$ under the constraint of the constant shear stress τ (31). Here $\mathbf{R} = (\vec{r}_1, \vec{r}_2, ..., \vec{r}_N)$ is the location of the packing in the configurational space with $\vec{r}_i$ $(i = 1, 2, ..., N)$ being the position of particle i, γ being the shear strain, and H being the appropriate enthalpy for sheared systems (*Materials and Methods*).

When the packing is perturbed from $(\mathbf{R}_0, \gamma_0)$ to $(\mathbf{R}_0, \gamma_0) + \lambda\mathbf{u}$, the energy can be expanded to

$$H(\lambda) = H_0 + \frac{1}{2}M^{(2)}\mathbf{u}^2\lambda^2 + \frac{1}{6}M^{(3)}\mathbf{u}^3\lambda^3 + \mathcal{O}(\lambda^4), = H_0 + \frac{1}{2}H''(0)\lambda^2 - \frac{1}{3}a_3\lambda^3 + \mathcal{O}(\lambda^4), \quad [5]$$

where $\mathbf{u} = (\vec{u}_1, \vec{u}_2, ..., \vec{u}_N, u_\gamma)$ is a normalized direction of particle displacements with $\vec{u}_i$ $(i = 1, 2, ..., N)$ being the displacement of particle i and u_γ being the variation of shear strain, $\lambda \ll 1$ is the magnitude of particle displacements, $H_0 = H(\mathbf{R}_0, \gamma_0)$ is the energy of the jammed packing, $M^{(2)}$ is the $(dN+1) \times (dN+1)$ Hessian matrix with d being the dimension of space, and $M^{(3)}$ is the $(dN+1) \times (dN+1) \times (dN+1)$ tensor quantifying the anharmonicity.

Eq. **5** is a general expansion of $H(\lambda)$ along arbitrary directions. If $\mathbf{u}$ is the direction approaching the instability, Eq. **5** is exactly Eq. **2** when $\lambda = x - x_0$. The frequency associated with the instability is thus expected to be $\omega_c = \sqrt{H''(0)}$. As shown in Eq. **5**, the frequency ω_c and the anharmonicity a_3 can be directly calculated from $M^{(2)}$ and $M^{(3)}$, respectively.

According to the fold instability, on approaching the instability, $\mathbf{u}$ follows the lowest normal mode of vibration $\mathbf{e}_m = (\vec{e}_1, \vec{e}_2, ..., \vec{e}_N, e_\gamma)$ with a frequency ω_m, so $\mathbf{u} = \mathbf{e}_m$ and $\omega_c = \omega_m$ (13), where $\vec{e}_i$ $(i = 1, 2, ..., N)$ is the polarization vector of particle i, and e_γ corresponds to the shear strain.

Fig. 1 *A–D* reviews the results for a fold instability for a two-dimensional (2D) system with the harmonic interaction potential (Eq. **10** in the *Materials and Methods* with $\alpha = 2$). As shown in Fig. 1*A*, on approaching the instability at τ_c, the shear-stress curve $\tau(\gamma)$ flattens out, indicating that the shear modulus approaches 0 at τ_c. Fig. 1*B* shows the frequency of the lowest normal mode, $\omega_m \sim (\delta\tau)^{1/4} = (\tau_c - \tau)^{1/4}$, as predicted in Eq. **3**. Fig. 1*C* shows that the normalized direction of the particle displacements $\mathbf{u}$ agrees with the lowest normal mode $\mathbf{e}_m$, demonstrated by $P_{ue} = |\mathbf{u}(\tau) \cdot \mathbf{e}_m(\tau)| \approx 1$. Fig. 1*C* also indicates that $P_{uu} = |\mathbf{u}(\tau) \cdot \mathbf{u}(\tau_c)| \approx 1$. Therefore, the instability develops in the direction of the lowest normal mode, which remains almost fixed, although $\omega_c = \omega_m$ varies significantly with $\delta\tau$. Fig. 1*D* shows that the computed energy barrier height along $\mathbf{u} = \mathbf{e}_m$ is $\Delta H = H(\lambda_b) - H_0 \sim (\delta\tau)^{3/2}$, consistent with Eq. **4**. Here λ_b is the minimum λ above which the minimization of H under constant shear stress τ can no longer drive the system back to $(\mathbf{R}_0, \gamma_0)$.

Results

Discontinuous Instabilities. Discontinuous instabilities look completely different from fold instabilities. Fig. 1 *E* and *F* shows that when $\delta\tau \to 0$, the stress $\tau(\gamma)$ remains linear and the frequency of the lowest vibrational mode, ω_m, approaches a nonzero constant. Therefore, there is no signature of the instability in either τ or ω_m. Moreover in Fig. 1*G*, although $P_{uu} \approx 1$, P_{ue} is significantly less than 1, so $\mathbf{u}$ remains almost constant, but does not follow the lowest normal mode. Fig. 1*H* shows that ΔH vanishes at τ_c with $\Delta H \sim (\delta\tau)^2$. This has a different scaling exponent from the 3/2-power found for fold instabilities.

We start with $n_t \approx 10{,}000$ jammed states at a given initial pressure and quasistatically shear them until the first instability occurs. The instabilities occur at different shear stresses τ_c for different states (13). Afterward, we classify the instabilities into fold and discontinuous ones according to their lowest-frequency behaviors and count the number of discontinuous instabilities n_d. The faction of discontinuous instabilities is thus $f = n_d/n_t$. For the harmonic repulsive potential, discontinuous instabilities far outnumber fold instabilities. For example, for 2D N = 1,024 systems initially at pressure $P = 0.05$, we find about 95.8% of the incipient instabilities are of the discontinuous type. With increasing N, the fraction of discontinuous instabilities decreases only slightly. Some results of the pressure and system size dependence of f and the distribution of τ_c are shown in *SI Appendix*.

Bond Breaking Triggers Discontinuous Instabilities. To find the origin of discontinuous instabilities, we compare in Fig. 2 *A* and *B* the energy $H(\lambda)$ with $H_a(\lambda)$, the third-order approximation

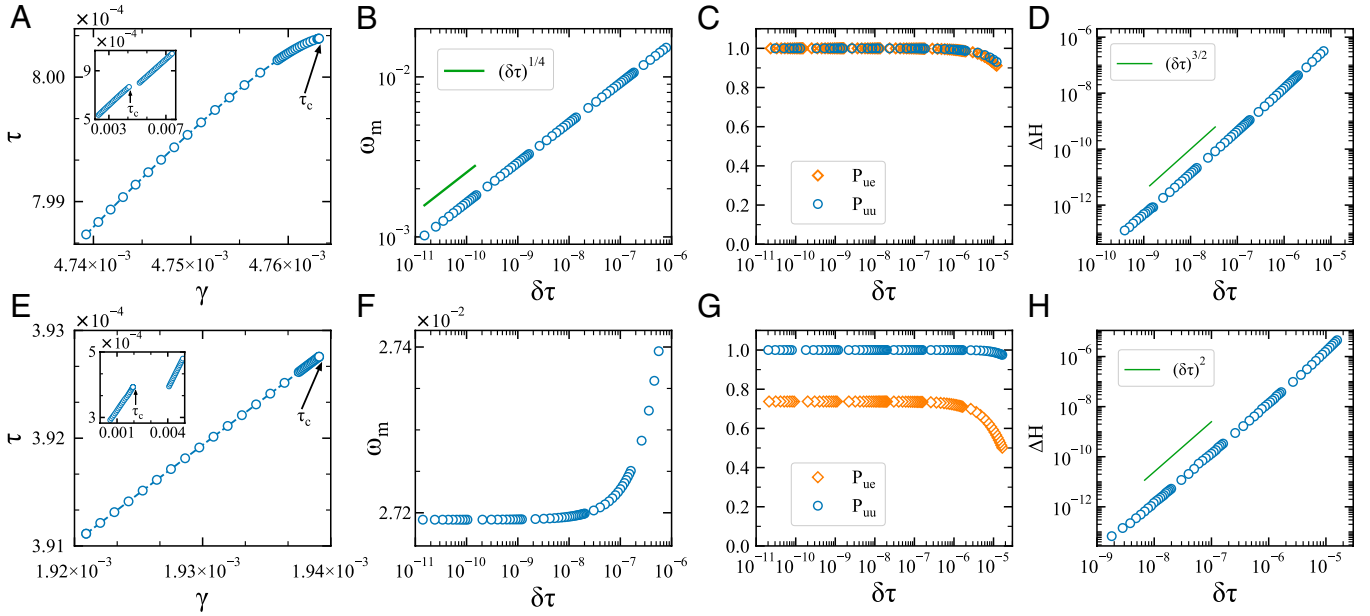

Fig. 1. Comparison of two types of instabilities under shear for 2D jammed packings of N = 1,024 particles interacting via the harmonic interaction potential initially at $P = 5 \times 10^{-2}$. Panels (*A–D*) and (*E–H*) are, respectively, for the fold instability and the discontinuous instability. (*A* and *E*) The shear stress, τ, is shown versus shear strain, γ, on approaching the instability. The insets show the results over a wider range of stress on both sides of the instability. (*B* and *F*) The frequency of the lowest normal mode of vibration, ω_m, is shown versus shear-stress distance from the instability, $\delta\tau \equiv (\tau_C - \tau)$. (*C* and *G*) The projections of the particle displacements onto the lowest normal mode, P_{ue}, and the particle displacements at the instability, P_{uu}, are shown versus $\delta\tau$. (*D* and *H*) The energy barrier height, ΔH, is shown versus $\delta\tau$.

of Eq. **5**, along $\mathbf{u} = \mathbf{u}(\tau_c)$ for the two types of instabilities. For both cases, we choose a local energy minimum $(\mathbf{R}_0, \gamma_0)$ which is $-\lambda_0\mathbf{u}$ away from the instability with $0 < \lambda_0 \ll 1$.

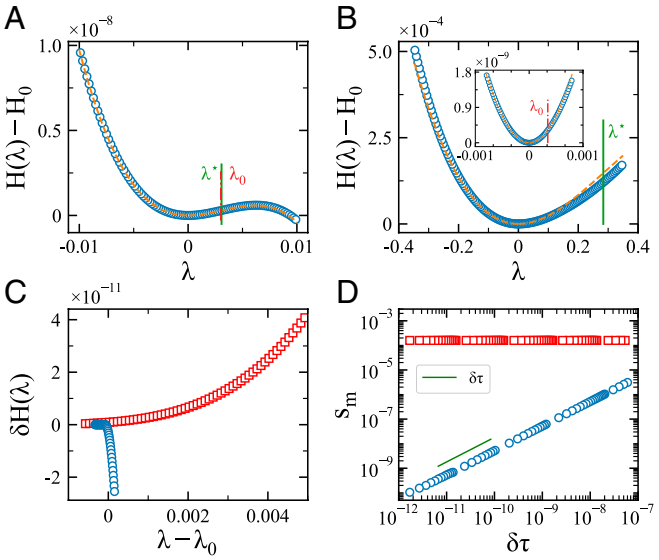

Fig. 2. Bond-breaking as the characteristic of the discontinuous instability. (*A* and *B*) Examples of the energy $H(\lambda)$ along the direction of the displacement field $\mathbf{u} = \mathbf{u}(\tau_C)$ at $\delta\tau = 1.2 \times 10^{-7}$ and 1.6×10^{-7} for the fold instability and the discontinuous instability, respectively. Both energies from the simulation and from the third-order approximation of Eq. **5**, $H(\lambda)$ (circles) and $H_a(\lambda)$ (dashed lines) are shown. The inset of (*B*) shows a zoom into a narrower range of λ near the minimum. The vertical solid and dot-dashed lines show the locations of λ^* and λ_0, where $H'' = 0$ and the instability happens, respectively. (*C*) Difference between $H(\lambda)$ and $H_a(\lambda)$, $\delta H(\lambda) = H(\lambda) - H_a(\lambda)$, for the fold instability (red squares) and the discontinuous instability (blue circles) shown in (*A*) and (*B*), respectively. (*D*) Minimum particle overlap $s_m(\delta\tau)$ on approaching the instability for the fold instability (red squares) and the discontinuous instability (blue circles).

From Eq. **5**, we have $H_a''(\lambda) = H''(0) - 2a_3\lambda$. When $\lambda = \lambda^* = H''(0)/2a_3$, $H_a''(\lambda^*) = 0$, so λ^* is the inflection point. For the fold instability, because $H''(0) = \omega_c^2$, $\lambda^* = \omega_c^2/2a_3 = -x_0$ from Eq. **3**. Note that $\lambda = x - x_0$. By definition, the instability happens at $x = 0$, so that $\lambda_0 = -x_0$. Therefore, $\lambda^* = \lambda_0$ for the fold instability. The instability can be predicted from the shape of $H_a(\lambda)$ of the jammed state at $(\mathbf{R}_0, \gamma_0)$: It corresponds to the vanishing of the local curvature of $H_a(\lambda)$ at $\lambda = \lambda^* = \lambda_0$.

Fig. 2*A* indicates that $H(\lambda)$ and $H_a(\lambda)$ agree well for the fold instability. The anharmonicity leads to an energy maximum corresponding to the energy barrier height and the continuous change of the local curvature. For such a case, $\lambda^* = \lambda_0$ is verified. However, Fig. 2*B* shows that λ_0 is much smaller than λ^* for the discontinuous instability, so that the instability happens when $H_a''(\lambda)$ is still positive and $H(\lambda)$ is still approximately harmonic. Because the shear modulus and $H''(0) = \omega_m^2$ remain constant on approaching the instability in this case (Fig. 1 *E* and *F*), $\delta\tau \sim \lambda_0$ and the energy barrier height $\Delta H \sim H''(0)\lambda_0^2 \sim (\delta\tau)^2$, explaining the scaling shown in Fig. 1*H*.

A closer look at the error, $\delta H(\lambda) = H(\lambda) - H_a(\lambda)$, unveils a further difference between the two types of instabilities. One would expect $|\delta H(\lambda)|$ to grow with increasing $\lambda - \lambda_0$ due to stabilizing higher order terms in Eq. **5**. Fig. 2*C* shows that indeed, $\delta H(\lambda)$ increases with λ for the fold instability (red points), but $\delta H(\lambda)$ decreases for the discontinuous instability (blue points).

Fig. 2*C* implies that the expansion of the energy in powers of λ in Eq. **5** must break down for discontinuous instabilities. Note that Eq. **5** perturbs around the force network at $(\mathbf{R}_0, \gamma_0)$. This expansion is valid when the topology of the force network does not change with the increase of λ. However, Eq. **5** should fail if the topology changes. With the continuous increase of λ and shift of particle positions, the simplest change of the topology is the breaking of a bond.

Fig. 2*D* verifies that the discontinuous instabilities are indeed accompanied by the breaking of a bond. We calculate the

relative particle overlap, s_{ij}, of interacting particles i and j (*Materials and Methods*) and find the minimum value s_m of all interacting particle pairs. On approaching the discontinuous instability (blue points), $s_m \sim \delta\tau$, so the bond breaks right at the instability. As a comparison, we also show $s_m(\delta\tau)$ for a fold instability (red points). It approaches a positive constant at the instability, showing that the topology of the force network remains unchanged.

Stabilizing Bonds. We have demonstrated that a bond is broken at a discontinuous instability. However, it is not guaranteed that breaking a bond will cause a discontinuous instability. In fact, it is well known that bonds can form or break in the absence of any instability (32–34). This leads us to the idea that there is a population of "stabilizing bonds," whose existence maintains mechanical stability of the system. Only the breaking of stabilizing bonds leads to discontinuous instabilities.

The identification of the stabilizing bonds is as follows. For a jammed packing obtained from the minimization of the energy H, we calculate its Hessian matrix. Then, we choose a bond to remove. That is to subtract the contributions of this bond from the elements of the Hessian matrix associated with the bond, while keeping all the other elements unchanged. If the diagonalization of the updated Hessian matrix results in a negative nontrivial eigenvalue, the bond is a stabilizing bond. Fig. 3*A* shows results for the jammed packing whose instability occurs at λ_0 in Fig. 2*B*. We repeat the above procedure for every bond and obtain the lowest eigenvalue ξ_m of the Hessian matrix. The removal of any single bond decreases ξ_m. However, for many bonds, ξ_m remains positive. Only a fraction of bonds leads to a negative ξ_m when removed, causing an instability, so these bonds are stabilizing bonds. Note that the lowest eigenvalue jumps discontinuously from $\xi_m > 0$ before the instability, as shown in Fig. 1*F*, where we plot $\omega_m = \sqrt{\xi_m}$, to $\xi_m < 0$ once the bond breaks. This is the discontinuity that justifies our naming of "discontinuous instabilities." Fig. 3 *A*, *Bottom* shows that, when any single bond is replaced with an unstressed bond with the original stiffness, no negative eigenvalues exist for the updated Hessian matrix. Therefore, stabilizing effect of stabilizing bonds does not depend on whether or not they are bearing force.

Fig. 3*B* shows the configuration and force network of the jammed packing that goes unstable. Stabilizing bonds are highlighted in red. As expected, the breaking bond that causes the discontinuous instability is one of the stabilizing bonds. We calculate the quantity (18)

$$\Psi_i = \sum_l \frac{1}{\omega_l^2} |\vec{e}_{i,l}|^2, \qquad [6]$$

for particle i (= 1, 2, ..., N), where ω_l and $\vec{e}_{i,l}$ are the frequency and the polarization vector of particle i of mode l, and the sum is over all nontrivial modes. It has been shown that Ψ_i is the response of the mean squared displacement of particle i to the increase of temperature (18, 35) and can thus be used to characterize particle softness in order to identify soft spots, i.e., particle clusters with higher tendency to rearrange under external perturbations. The higher Ψ is, the softer the particle behaves. In Fig. 3*B*, particles with top 10% Ψ values are highlighted in dark blue. Interestingly, they show strong spatial correlations with the stabilizing bonds. Because Ψ is a reasonable predictor of rearrangements under load (16, 17, 36–39), we expect that stabilizing bonds should also be useful predictors. Stabilizing bonds are a predictor and, as we show below, generally exist for other potentials.

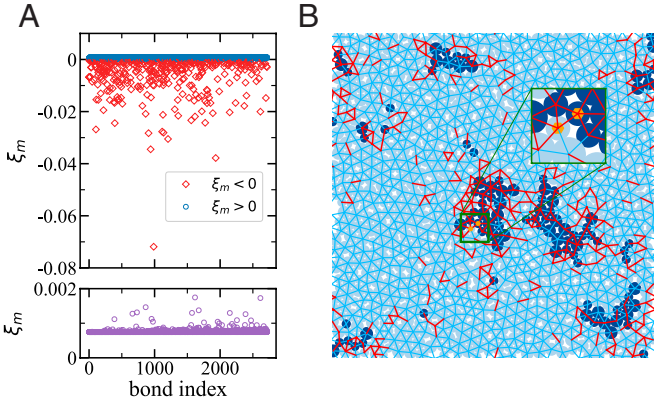

Fig. 3. Identification of stabilizing bonds. (*A*) Values of the lowest eigenvalue of the Hessian matrix, ξ_m, when a bond is removed (*Top*). When a stabilizing bond is removed, the system develops a negative eigenvalue (shown in red) and is unstable. Removal of nonstabilizing bonds leaves $\xi_m > 0$ (shown in blue) and the packing stable. When the bonds are replaced by an unstressed one of the same stiffness (*Bottom*), the system does not develop any negative eigenvalues and remains stable. The criterion for whether a bond is a stabilizing bond, therefore, does not depend on whether or not it is under stress. The results are for the jammed packing discussed in Fig. 2*B*, which is $-\lambda_0\mathbf{u}$ away from the instability. (*B*) Configuration of the jammed packing with the force network. Stabilizing bonds are in red. The light blue bonds are nonstabilizing ones. The bond whose breaking leads to the instability at τ_c is highlighted by the orange dots. Softest particles with top 10% Ψ values are highlighted in dark blue.

Evolution from Fold Instability to Discontinuous Instability with Bond Stiffness. Until now, we have concentrated on packings with the harmonic potential. As seen from Eq. **10** in *Materials and Methods*, the harmonic potential with $\alpha = 2$ has a bond stiffness, i.e., the second derivative of the interaction potential U'', which is constant independent of the particle overlap s_{ij}. As a result, when a bond is about to break ($s_{ij} \to 0$) and the force is vanishing, the existence of the bond still contributes to the Hessian matrix and maintains the stability of the system, because $U'' > 0$. However, the Hertzian potential (Eq. **10** with $\alpha = 5/2$ and $s_c = 0$) does not have this property; U'' decreases with the decrease of s_{ij} and vanishes when $s_{ij} = 0$. When a bond is breaking, both the force and bond stiffness tend to vanish, and so does its contribution to the Hessian matrix. Therefore, for the Hertzian potential, a bond can be a stabilizing bond only when it bears force. Because breaking such a bond is necessary for the discontinuous instability to occur, it is expected that there are no discontinuous instabilities for jammed packings with the Hertzian potential.

Another question is whether discontinuous instabilities can occur whenever $U'' > 0$ at the potential cutoff, no matter how small U'' is. To address this, we truncate the Hertzian potential by using a potential cutoff $s_c > 0$ as shown in Eq. **10**. Clearly, $U''(s_c)$ increases with s_c. Fig. 4*A* shows the fraction of discontinuous instabilities, $f(s_c)$, as a function of s_c, for 2D jammed packings of $N = 256$ Hertzian particles. For small s_c, $f(s_c)$ increases as a power law with $f \sim s_c^{0.44}$. It saturates to almost 1 when s_c is above 10^{-2}. Therefore, discontinuous instabilities occur as long as U'' is nonvanishing at the potential cutoff, with the fraction of instabilities that are discontinuous increasing with s_c. For the harmonic potential, U'' remains constant regardless of the particle overlap, corresponding to the large s_c behavior of $f(s_c)$ shown in Fig. 4*A*, consistent with our finding that discontinuous instabilities far outnumber fold instabilities.

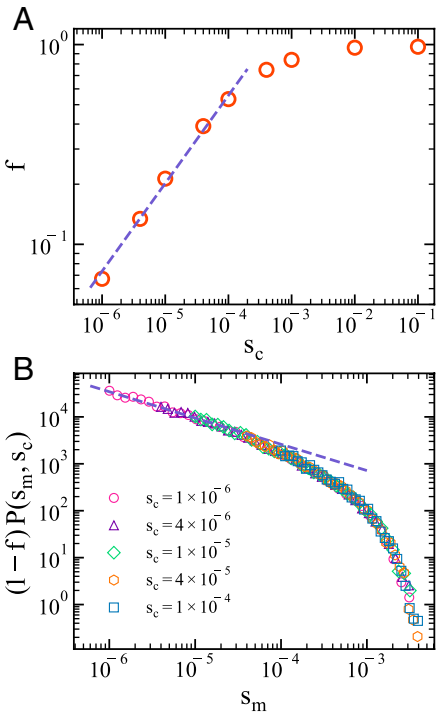

Fig. 4. Nonvanishing bond stiffness at the potential cutoff leads to discontinuous instabilities. (*A*) Fraction of discontinuous instabilities as a function of s_c as defined in the text, $f(s_c)$, for 2D jammed packings of $N = 256$ Hertzian particles interacting via the potential shown in Eq. **10** initially generated at $p = 8 \times 10^{-3}$. The dashed line shows the power law scaling, $f \sim s_c^{0.44}$. (*B*) Collapse of the distribution $P(s_m, s_c)$ for the fold instability multiplied by $(1-f)$. The dashed line shows the power law scaling, $P(s_m, 0) \sim s_m^{-0.56}$.

To understand the scaling of $f(s_c)$ at small values of s_c, we show in Fig. 4*B* the probability distribution of the smallest particle overlap s_m, $P(s_m, s_c)$, for fold instabilities. Interestingly, all curves at small values of s_c collapse well when we multiply $P(s_m, s_c)$ by $1-f(s_c)$. Because $f(0) = 0$ and s_m cannot be smaller than s_c by definition, the collapse implies

$$[1-f(s_c)]P(s_m, s_c) = P(s_m, 0)\Theta(s_m - s_c), \qquad [7]$$

where $\Theta(x)$ is the Heaviside step function. The master curve is the distribution for $s_c = 0$, $P(s_m, 0)$, which shows a power law behavior at small values of s_m: $P(s_m, 0) \sim s_m^{-0.56}$. By definition,

$$1-f(s_c) = \int_{s_c}^{1} ds_m P(s_m, 0) = 1 - \int_{0}^{s_c} ds_m P(s_m, 0). \qquad [8]$$

As a result,

$$f(s_c) = \int_{0}^{s_c} ds_m P(s_m, 0) \sim \int_{0}^{s_c} ds_m s_m^{-0.56} \sim s_c^{0.44}, \qquad [9]$$

as long as s_c lies in the power-law regime of $P(s_m, 0)$. Therefore, the collapse in Fig. 4*B* indicates that more and more fold instabilities with $s_m < s_c$ convert into discontinuous instabilities with increasing s_c, leading to the growth of $f(s_c)$.

General Existence of Stabilizing Bonds. Stabilizing bonds are not unique to special potentials with nonvanishing stiffness like the harmonic potential. They generally exist in disordered solids. In Fig. 5, we show examples for the Hertzian potential ($s_c = 0$) and the inverse-power-law potential with a vanishing stiffness at the potential cutoff. For both cases, stabilizing bonds comprise a significant fraction of the total.

Fig. 5 also shows that spatial correlations between stabilizing bonds and soft spots are also strong for both cases. Therefore, the stabilizing bonds are in fact general indicators of local stability and predictors of mechanical failure for disordered solids.

Discussion

Bonds commonly break when disordered solids are subjected to increasing mechanical loads (32–34). We have shown here an overlooked type of instability; compared with the widely accepted fold instability, this instability exhibits discontinuous features. In particular, it has a nonvanishing elastic modulus and nonvanishing frequency of the lowest normal mode of vibration. We have demonstrated that discontinuous instabilities will occur as long as the bond stiffness is nonzero at the potential cutoff. These findings enrich our understanding of mechanical instabilities of disordered solids and explain why the harmonic repulsive potential produces such different behavior from, e.g., Hertzian interaction near an instability. While it is not a good model for studying the behavior of systems under load with a vanishing stiffness at the potential cutoff, the harmonic repulsive potential is a model, commonly used, especially in the development of the physics of jamming (20), that highlights how a different kind of instability can occur in disordered solids.

The harmonic repulsive potential is also a good approximation to the interaction for a number of systems studied in the laboratory such as granular materials (26, 27) and emulsions (28, 29), which interact via contact forces. Theoretical studies also suggest that the interaction between elastic bodies is harmonic in both two and three dimensions, while in three dimensions there are logarithmic corrections, which are imperceptible except when particle overlap is extremely small (40–43). Therefore, the discontinuous instability is not limited to studies based on simulation; it has theoretical support and should be observed in some laboratory systems. Moreover, our study implies that discontinuous instabilities may occur when there is a discontinuous drop of the bond stiffness, irrespective of whether or not the discontinuity is at the potential cutoff. We expect that the strength of the bond stiffness discontinuity, e.g., the ratio of the magnitude of the drop to the stiffness before/after the drop, may act as a control parameter for the probability of discontinuous instabilities.

Our understanding of discontinuous instabilities rests on the finding of stabilizing bonds. Such bonds exist for disordered solids with arbitrary potentials and are spatially correlated with

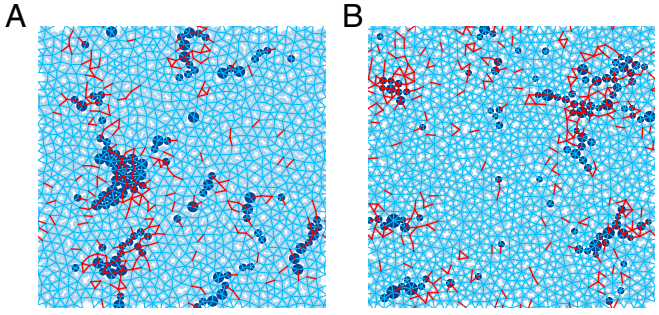

Fig. 5. Spatial correlations between stabilizing bonds and soft spots in (*A*) Hertzian and (*B*) inverse-power-law potentials at $P = 0.01$ and 3, respectively. As in Fig. 3*B*, the particles with the *Top* 10% of Ψ values are highlighted in dark blue. Stabilizing bonds are red and nonstabilizing bonds are light blue.

soft spots. In previous studies, soft spots have been used to predict the locations of mechanical failure and the corresponding particle rearrangements under load (15–17, 44). Therefore, we expect stabilizing bonds to have similar predictive power. The identification of stabilizing bonds has the advantage of being clean: removal of a stabilizing bond produces a negative eigenvalue of the Hessian matrix. This is in sharp contrast to the definition of soft spots, which usually requires a threshold of Ψ. It is therefore important to determine systematically whether these bonds are in fact good, or possibly even better, predictors of particle rearrangements than previously proposed quantities. Because these bonds are crucial to the stability of disordered solids, they might also play a significant role in characterizing the unusual elastic and vibrational properties of disordered solids.

Materials and Methods

Our systems consist of N frictionless particles with the same mass m in a cubic box with side length L. In the absence of shear, periodic boundary conditions are applied in all directions. In the case of shear, Lees–Edwards boundary conditions (45) are used.

We mainly consider the pairwise interaction potential

$$U(r_{ij}) = \frac{\epsilon}{\alpha} s_{ij}^{\alpha} \Theta\left(s_{ij} - s_c\right), \qquad [10]$$

where $s_{ij} = 1 - r_{ij}/\sigma_{ij}$ quantifies the particle overlap with r_{ij} and σ_{ij} being the separation between particles i and j and sum of their radii, respectively, ϵ is the characteristic energy, $\Theta(x)$ is the Heaviside step function, and $s_c \geq 0$ sets the cutoff of the potential. We shift the potential to have $U = U' = 0$ when $s_{ij} = s_c$. When $\alpha = 2$ or $5/2$, Eq. **10** describes the harmonic or Hertzian potential. For harmonic potential, we set $s_c = 0$. The bond stiffness $U'' = \epsilon/\sigma_{ij}^2 > 0$, independent of particle overlap s_{ij}. For Hertzian potential, we vary s_c in order to study how the bond stiffness U'' at the potential cutoff affects the results, so $U'' = \frac{3}{2}\frac{\epsilon}{\sigma_{ij}^2} s_c^{1/2}$ increases when s_c increases. To avoid crystallization, we use binary mixtures with $N/2$ large and $N/2$ small spherical particles for both harmonic and Hertzian potentials. The diameters of large and small particles are 1.4σ and σ, respectively.

We also show some results for the inverse-power-law potential, $U(r_{ij}) = \epsilon(\sigma_{ij}/r_{ij})^{12}$, truncated at $r_{ij} = r_c = 1.25\sigma_{ij}$. We shift the potential to guarantee that $U(r_c) = U'(r_c) = U''(r_c) = 0$. For the inverse-power-law potential, the diameter of particle i is extracted from a continuous probability distribution $P(\sigma_i) = A\sigma_i^{-3}$ with A being the normalization factor. The average diameter is σ. To avoid crystallization, we use a nonadditive mixing rule to set σ_{ij}: $\sigma_{ij} = \frac{1}{2}(\sigma_i + \sigma_j)(1 - 0.2|\sigma_i - \sigma_j|)$ (46, 47).

For all systems, the units of length, mass, and energy are σ, m, and ϵ. The frequency has units of $\sqrt{\epsilon/m\sigma^2}$.

We first generate jammed packings at a given pressure p by instantaneously quenching high-temperature states to local enthalpy minima via the fast inertial relaxation engine (FIRE) algorithm (48). We perform quasistatic shear to a jammed packing by increasing the shear stress τ while minimizing the enthalpy-like energy $H(R, \gamma) = U_t - \tau\gamma L^d$ via FIRE (31), until there is an abrupt change of γ at $\tau = \tau_c$ corresponding to the instability (13). Here U_t is the total potential energy, γ is the shear strain, and d is the dimension of space. For compression, we successively increase the pressure and minimize the enthalpy until an instability at $p = p_c$ occurs.

The normal modes of vibration can be obtained from the diagonalization of the Hessian matrix associated with the energy $H(R, \gamma)$. In this work, we are mainly concerned about the nontrivial mode with the lowest nonzero eigenvalue.

Data, Materials, and Software Availability. All study data are included in the article and/or *SI Appendix*.

ACKNOWLEDGMENTS. This work was supported by the National Natural Science Foundation of China Grants No. 12074355 and No. 11734014 (N.X.), the Simons Foundation for the collaboration Cracking the Glass Problem via awards 454945 (A.J.L.), 348126 (S.R.N.), and Investigator Award 327939 (A.J.L.). The Flatiron Institute is a division of the Simons Foundation. We also thank the Supercomputing Center of University of Science and Technology of China for the computer time.

1. D. L. Malandro, D. J. Lacks, Volume dependence of potential energy landscapes in glasses. *J. Chem. Phys.* **107**, 5804 (1997).
2. D. J. Lacks, Localized mechanical instabilities and structural transformations in silica glass under high pressure. *Phys. Rev. Lett.* **80**, 5385 (1998).
3. D. L. Malandro, D. J. Lacks, Relationships of shear-induced changes in the potential energy landscape to the mechanical properties of ductile glasses. *J. Chem. Phys.* **110**, 4593 (1999).
4. C. E. Maloney, A. Lemaître, Subextensive scaling in the athermal, quasistatic limit of amorphous matter in plastic shear flow. *Phys. Rev. Lett.* **93**, 016001 (2004).
5. C. E. Maloney, A. Lemaître, Universal breakdown of elasticity at the onset of material failure. *Phys. Rev. Lett.* **93**, 195501 (2004).
6. C. E. Maloney, A. Lemaître, Amorphous systems in athermal, quasistatic shear. *Phys. Rev. E* **74**, 016118 (2006).
7. M. Tsamados, A. Tanguy, C. Goldenberg, J.-L. Barrat, Local elasticity map and plasticity in a model Lennard-Jones glass. *Phys. Rev. E* **80**, 026112 (2009).
8. A. Tanguy, B. Mantisi, M. Tsamados, Vibrational modes as a predictor for plasticity in a model glass. *Europhys. Lett.* **90**, 16004 (2010).
9. N. Xu, V. Vitelli, A. J. Liu, S. R. Nagel, Anharmonic and quasi-localized vibrations in jammed solids-Modes for mechanical failure. *Europhys. Lett.* **90**, 56001 (2010).
10. B. Mantisi, A. Tanguy, G. Kermouche, E. Barthel, Atomistic response of a model silica glass under shear and pressure. *Eur. Phys. J. B* **85**, 304 (2012).
11. L. Gartner, E. Lerner, Nonlinear plastic modes in disordered solids. *Phys. Rev. E* **93**, 011001(R) (2016).
12. E. Lerner, Micromechanics of nonlinear plastic modes. *Phys. Rev. E* **93**, 053004 (2016).
13. N. Xu, A. J. Liu, S. R. Nagel, Instabilities of jammed packings of frictionless spheres under load. *Phys. Rev. Lett.* **119**, 215502 (2017).
14. A. Nicolas, E. E. Ferrero, K. Martens, J.-L. Barrat, Deformation and flow of amorphous solids: Insights from elastoplastic models. *Rev. Mod. Phys.* **90**, 045006 (2018).
15. M. L. Manning, A. J. Liu, Vibrational modes identify soft spots in a sheared disordered packing. *Phys. Rev. Lett.* **107**, 108302 (2011).
16. K. Chen *et al.*, Measurement of correlations between low-frequency vibrational modes and particle rearrangements in quasi-two-dimensional colloidal glasses. *Phys. Rev. Lett.* **107**, 108301 (2011).
17. J. Ding, S. Patinet, M. L. Falk, Y. Cheng, E. Ma, Soft spots and their structural signature in a metallic glass. *Proc. Natl. Acad. Sci. U.S.A.* **111**, 14052 (2014).
18. H. Tong, N. Xu, Order parameter for structural heterogeneity in disordered solids. *Phys. Rev. E* **90**, 010401(R) (2014).
19. P. G. Debenedetti, F. H. Stillinger, Supercooled liquids and the glass transition. *Nature* **410**, 259–267 (2001).
20. A. J. Liu, S. R. Nagel, The jamming transition and the marginally jammed solid. *Annu. Rev. Condens. Matter Phys.* **1**, 347 (2010).
21. P. Charbonneau, J. Kurchan, G. Parisi, P. Urbani, F. Zamponi, Fractal free energy landscapes in structural glasses. *Nat. Commun.* **5**, 3725 (2014).
22. Y. Jin, H. Yoshino, Exploring the complex free-energy landscape of the simplest glass by rheology. *Nat. Commun.* **8**, 14935 (2017).
23. Y. Jin, P. Urbani, F. Zamponi, H. Yoshino, A stability-reversibility map unifies elasticity, plasticity, yielding, and jamming in hard sphere glasses. *Sci. Adv.* **4**, eaat6387 (2018).
24. J. Zhang et al., Unifying fluctuation-dissipation temperatures of slow-evolving nonequilibrium systems from the perspective of inherent structures. *Sci. Adv.* **7**, eabg6766 (2021).
25. V. Arnold, *Catastrophe Theory* (Springer-Verlag, Berlin, ed. 3, 1992).
26. T. S. Majmudar, M. Sperl, S. Luding, R. P. Behringer, Jamming transition in granular systems. *Phys. Rev. Lett.* **98**, 058001 (2007).
27. C. Coulais, A. Seguin, O. Dauchot, Shear modulus and dilatancy softening in granular packings above jamming. *Phys. Rev. Lett.* **113**, 198001 (2014).
28. T. G. Mason, J. Bibette, D. A. Weitz, Elasticity of compressed emulsions. *Phys. Rev. Lett.* **75**, 2051 (1995).
29. M.-D. Lacasse, G. S. Grest, D. Levine, T. G. Mason, D. A. Weitz, Model for the elasticity of compressed emulsions. *Phys. Rev. Lett.* **76**, 3448 (1996).
30. S. Dagois-Bohy, B. P. Tighe, J. Simon, S. Henkes, M. van Hecke, Soft-sphere packings at finite pressure but unstable to shear. *Phys. Rev. Lett.* **109**, 095703 (2012).
31. H. Liu, X. Xie, N. Xu, Finite size analysis of zero-temperature jamming transition under applied shear stress by minimizing a thermodynamic-like potential. *Phys. Rev. Lett.* **112**, 145502 (2014).
32. M. S. van Deen et al., Contact changes near jamming. *Phys. Rev. E* **90**, 020202(R) (2014).
33. P. Wang *et al.*, Shear response of granular packings compressed above jamming onset. *Phys. Rev. E.* **103**, 022902 (2021).
34. P. Morse, S. Wijtmans, M. van Deen, M. van Hecke, M. L. Manning, Differences in plasticity between hard and soft spheres. *Phys. Rev. Res.* **2**, 023179 (2020).
35. H. Tong, H. Hu, P. Tan, N. Xu, H. Tanaka, Revealing inherent structural characteristics of jammed particulate packings. *Phys. Rev. Lett.* **122**, 215502 (2019).
36. J. Rottler, S. S. Schoenholz, A. J. Liu, Predicting plasticity with soft vibrational modes: From dislocations to glasses. *Phys. Rev. E* **89**, 042304 (2014).

37. R. L. Jack, A. J. Dunleavy, C. P. Royall, Information-theoretic measurements of coupling between structure and dynamics in glass formers. *Phys. Rev. Lett.* **113**, 095703 (2014).
38. E. D. Cubuk *et al*., Identifying structural flow defects in disordered solids using machine-learning methods. *Phys. Rev. Lett.* **114**, 108001 (2015).
39. S. S. Schoenholz, E. D. Cubuk, D. M. Sussman, E. Kaxiras, A. J. Liu, A structural approach to relaxation in glassy liquids. *Nat. Phys.* **12**, 469 (2016).
40. D. C. Morse, T. A. Witten, Droplet elasticity in weakly compressed emulsions. *Europhys. Lett.* **22**, 549 (1993).
41. D. Weaire, R. Höhler, S. Hutzler, Bubble-bubble interactions in a 2D foam, close to the wet limit. *Adv. Colloid Interface Sci.* **247**, 491–495 (2017).
42. R. Höhler, S. Cohen-Addad, Many-body interactions in soft jammed materials. *Soft Matter* **13**, 1371–1383 (2017).
43. R. Höhler, D. Weaire, Can liquid foams and emulsions be modeled as packings of soft elastic particles? *Adv. Colloid Interface Sci.* **263**, 19–37 (2019).
44. A. Widmer-Cooper, H. Perry, P. Harrowell, D. R. Reichman, Irreversible reorganization in a supercooled liquid originates from localized soft modes. *Nat. Phys.* **4**, 711 (2008).
45. M. P. Allen, D. J. Tildesley, *Computer Simulation of Liquids* (Oxford University Press, New York, 1987).
46. L. Berthier, P. Charbonneau, A. Ninarello, M. Ozawa, S. Yaida, Zero-temperature glass transition in two dimensions. *Nat. Commun.* **10**, 1508 (2019).
47. A. Ninarello, L. Berthier, D. Coslovich, Models and algorithms for the next generation of glass transition studies. *Phys. Rev. X* **7**, 021039 (2017).
48. E. Bitzek, P. Koskinen, F. Gähler, M. Moseler, P. Gumbsch, Structural relaxation made simple. *Phys. Rev. Lett.* **97**, 170201 (2006).